

J-VAR: the northern variable sky in 7 filters

First Data Release

A. Ederoclit¹, H. Vázquez Ramió¹, A. Alvarez-Candal², B. B. Siffert³, V. M. Placco⁴, D. Morate¹, S. Pyrzas¹, C. López-Sanjuan¹, M. Mahlke⁵, S. Kulkarni¹, L. Espinosa⁶, M. J. Castro^{7,8}, B. Zacarias⁶, M. Akhlaghi¹, J. Castillo¹, T. Civera¹, J. Hernández-Fuertes¹, A. Hernán-Caballero¹, A. López-Sainz¹, G. Lorenzetti¹, D. Muniesa-Gallardo¹, A. Moreno-Signes¹, H. Vives-Arias¹, J. Zaragoza Cardiel¹, M. C. Díaz-Martín¹, F. Galindo-Guil¹, R. Iglesias-Marzoa¹, R. Infante-Sainz¹, T. Kuutma¹, E. Lacruz^{1,9}, J. Lamadrid-Gutierrez¹, F. López-Martínez¹, N. Maícas-Sacristan¹, F. Hernández Pérez⁹, J. Carvano¹⁰, P. Cruz¹¹, F. R. Herpich¹², E. Solano¹¹, A. F. Pala¹³, R. R. R. Reis³

¹ Centro de Estudios de Física del Cosmos de Aragón
e-mail: aederoc1@cefca.es

² Instituto de Astrofísica de Andalucía, CSIC, Apt 3004, E18080 Granada, Spain

³ Universidade Federal de Rio de Janeiro

⁴ NSF NOIRLab, Tucson, AZ 85719, USA

⁵ Université Marie et Louis Pasteur, CNRS, Institut UTINAM (UMR 6213), équipe Astro, F-25000 Besançon, France

⁶ Department of Astronomy, Instituto de Astronomia, Geofísica e Ciências Atmosféricas, Universidade de São Paulo

⁷ Fakultät für Physik und Astronomie, Universität Heidelberg, Im Neuenheimer Feld 226, D-69120 Heidelberg, Germany

⁸ Landessternwarte, Zentrum für Astronomie der Universität Heidelberg, Königstuhl 12, D-69117 Heidelberg, Germany

⁹ Universidad Internacional de Valencia (VIU), C/Pintor Sorolla 21, 46002 Valencia, Spain

¹⁰ Observatorio Nacional

¹¹ Centro de Astrobiología (CAB), CSIC-INTA, Camino Bajo del Castillo s/n, E-28692, Villanueva de la Cañada, Madrid, Spain.

¹² Laboratório Nacional de Astrofísica (LNA/MCTI), Rua Estados Unidos, 154, Itajubá 37504-364, Brazil

¹³ European Southern Observatory

Received ...; accepted ...

ABSTRACT

Aims. The analysis of variability of astronomical sources is of extraordinary interest, as it allows the study of astrophysical phenomena in real time. This paper presents the Javalambre Variability Survey (J-VAR) which leverages the narrow band filters available at the Javalambre Auxiliary Survey Telescope (JAST80) at the Observatorio Astrofísico de Javalambre (OAJ).

Methods. The JAST80 equipped with T80Cam, providing a field of view of 2 square degrees and a pixel scale of 0.55 arcsec/pixel has been designed for wide-field studies. The main characteristic is the availability of a variety of narrow band filters strategically located on stellar spectral features (the J0395 in correspondence of the Ca H+K doublet, the J0515 of the Mg b triplet, the J0660 of the H α line, and the J0861 of the Ca triplet). This project combines, for the first time, the wide-field with a variety of narrow band filters for a unique variability survey, observing each field 11 times with a standardised observing sequence. The median limiting magnitude for individual exposures are 19.1 mag in J0395 and J0515, 19.6 mag in J0660 and J0861, 19.8 mag in *i*, and 20.2 in *g* and *r*. The typical FWHM of the *r*-band images is 1.5 arcsec.

Results. This article introduces the first data release of J-VAR including more than 6000 individual asteroids, 10 detected optical transients (4 discovered supernovae), and 1.3 million light curves of point-sources. On average, J-VAR delivers an unprecedented ~5000 light curves per square degree of 11 epochs in 7 bands, opening research opportunities for theoretical studies and new discoveries alike.

Key words. Astronomical instrumentation, methods and techniques – Surveys – Minor planets, asteroids: general – (Stars:) binaries: general – Stars: variables: RR Lyrae – supernovae: general

1. Introduction

Variability is a fundamental property of the Universe, offering key insights across all spatial and temporal scales. From the pioneering use of Cepheid pulsations to establish the extragalactic distance scale (e.g., Leavitt & Pickering 1912; Hubble 1929), to the discovery of exoplanets through periodic variations in stellar brightness (e.g., Mayor & Queloz 1995), the study of time-dependent phenomena has continually transformed the field of astrophysics.

In recent years, the field of time-domain astrophysics has entered a golden era, driven by the start of several high-cadence (one day) photometric surveys. Ground-based projects such as All-Sky Automated Survey for Supernovae (ASAS-SN; Shappee et al. 2014), Catalina Real-time Transient Survey (CRTS; Drake et al. 2009), and Zwicky Transient Facility (ZTF; Bellm et al. 2019), operating mostly in up to three broadband filters, have mapped vast swathes of the sky, revealing countless new transients and variable sources. In parallel, space missions like the Convection Rotation and Transits satellite (CoRoT; Auvergne et al. 2009), *Kepler* (Borucki et al. 2010), the Transiting Exo-

planet Survey Satellite (TESS; Ricker et al. 2015), and *Gaia* (Gaia Collaboration et al. 2023) have provided light curves of exquisite precision for millions of sources, albeit typically in a single passband or pseudo-filter. Currently, the Vera C. Rubin Observatory is starting the Large Survey of Space and Time which is expected to deliver millions of alerts of transients per night covering the full sky every few nights with a dedicated 8 m telescope with 6 filters (Ivezić et al. 2019a).

Photometric monitoring in a single filter enables the detection and characterization of variability — amplitudes, timescales, and periodicities — but limits our understanding of the physical mechanisms at play. Spectroscopic time-domain follow-up adds the much-needed context of temperature, velocity, and chemical composition changes, but is observationally expensive and limited to small samples. An intermediate approach, increasingly explored in recent years, is time-domain photometry in multiple filters. This strategy combines the temporal cadence of imaging surveys with the spectral diagnostic power of multi-band photometry, allowing variability to be tracked not just in brightness, but across the spectral energy distribution (SED). Large-scale projects such as the Javalambre Photometric Local Universe Survey (J-PLUS; Cenarro et al. 2019) and the Javalambre-Physics of the Accelerating Universe Astrophysical Survey (J-PAS; Benitez et al. 2014; Bonoli et al. 2021) have demonstrated the power of this approach for static sky studies, using a combination of broad and narrow-band filters to recover low-resolution SEDs for millions of sources.

The Javalambre Variability Survey (J-VAR) builds on this legacy by bringing the multi-filter strategy into the time domain. Carried out with the JAST80, J-VAR employs a unique seven-filter system — three broad-band (g , r , i) and four narrow-band ($J0395$, $J0515$, $J0660$, and $J0861$) — to repeatedly observe each field 11 times. Designed to operate during conditions not suitable for the J-PLUS survey (e.g. poor seeing, bright sky background), J-VAR is unveiling the temporal evolution of stars, compact binaries, Solar System objects and optical transients with both cadence and spectral coverage.

The goal of this paper is to introduce J-VAR, its motivation, and to demonstrate its scientific potential. This paper is outlined as follows: Sect. 2 describes in detail the technical aspects and observing strategy of J-VAR, followed by an overview of the data reduction in Sect. 3. The First Data Release (DR1) of J-VAR is described in Sect. 4 and its main scientific drivers (including early results) in Sect. 5. Our conclusions and perspectives are outlined in Sect. 6.

A series of companion papers will offer further insights into different aspects of the survey and the data release, including the construction of calibrated light curves and variability indices (Pyrzas et al., submitted), the catalogue of minor bodies (Morate et al., submitted), and the light-curve fitting of RR Lyrae stars (Kulkarni et al., submitted).

Magnitudes are in the AB system (Oke & Gunn 1983), unless noted otherwise.

2. Observations

J-VAR is a multi-band time-domain survey of the northern sky designed to study variability in sky regions previously observed by the J-PLUS survey. By targeting the same fields using identical instrumentation, J-VAR leverages J-PLUS’s robust photometric calibration (López-Sanjuan et al. 2024) and other survey products that have matured over time, including source classifications (López-Sanjuan et al. 2019; del Pino et al. 2024) and

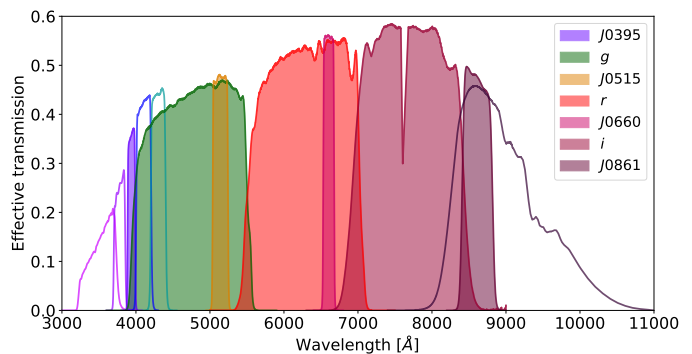


Fig. 1. The J-VAR filter set (shown as filled curves) is a subset of the J-PLUS photometric system (empty and filled curves). The effective transmission accounts for the CCD quantum efficiency, the filters measured transmission and the reflectivity of the primary and secondary mirror of JAST80.

photometric redshifts for extragalactic objects. The current J-VAR photometric calibration (Pyrzas et al. submitted; Morate et al. submitted) directly depends on the one of the J-PLUS third data release (J-PLUS DR3; López-Sanjuan et al. 2024). For this reason the J-VAR pointings follow the J-PLUS field definitions.

The main driver behind the choice of the filters of J-VAR is efficiency. Six filters (g , r , i , $J0515$, $J0660$, and $J0861$) have been chosen for being the most efficient filters (i.e. highest effective transmission of the whole system) of the J-PLUS filter-set, as it can be seen in Fig. 1. The $J0395$ has also been included to study the variation of the Ca H+K doublet, which is specially sensible to e.g. stellar chromospheric activity.

Observations are carried out at the OAJ (Cenarro et al. 2014) with the T80Cam panoramic camera attached to the Javalambre Auxiliary Survey Telescope (JAST80) (Marín-Franch et al. 2012, 2015). JAST80 is an 83 cm, f/4.5 modified Ritchey-Chrétien reflector on a German equatorial mount. The telescope and camera provide a pixel scale of 0.556 arcsec/pix and a $1.4 \text{ deg} \times 1.4 \text{ deg}$ (2 deg^2) field-of-view (FoV) that, on average, allows the detection of a number of sources of the order of 10^4 per individual image. J-VAR uses a subset of the J-PLUS photometric system (see Fig. 1). The latter was devised to measure some of the most prominent atmospheric stellar features with the aim of studying a wide variety of phenomena in the local Universe (for more details see Cenarro et al. 2019).

J-VAR’s observations started in May 2017, shortly after the beginning of the scientific operation of the JAST80/T80Cam, as a filler program running on non-photometric nights, whenever J-PLUS or other competitive open time programs demanding photometric conditions could not be executed. From 2019 to the end of 2022, J-VAR has been granted with competitive open time offered every semester by the OAJ as a large program. Since 2023 the survey continued, again as a filler program, as it did in the beginning. The evolution of the survey is shown in Fig. 2.

2.1. Observing strategy

The filler program nature of J-VAR necessitates consideration of potential cloud cover during observations. J-VAR targets a limiting magnitude ~ 1 mag brighter than J-PLUS, conducted with identical instrumentation including telescope, camera and filters. Non-photometric conditions cannot be modelled reliably, so bright time is used as the closest operational proxy in the ex-

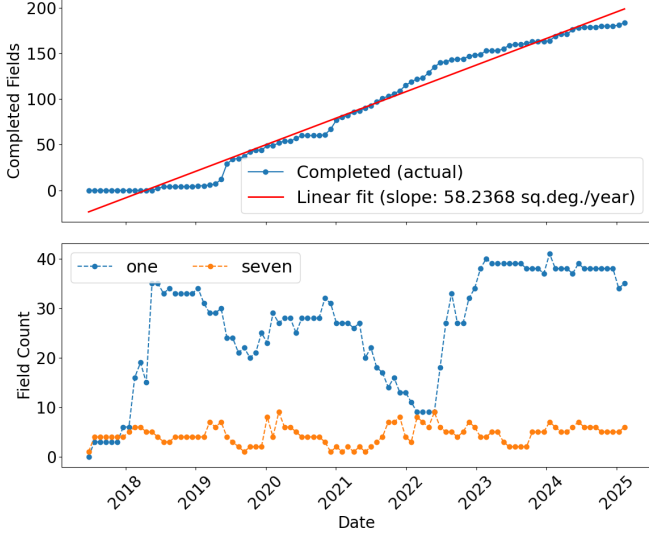


Fig. 2. Evolution of the observations of J-VAR. The upper panel shows the number of completed fields (i.e. fields with at least 11 observed epochs). The bottom panel shows the number of fields which have been observed one or seven times (the rest has been omitted for clarity). The number of fields with one observed epoch shows that there is a continuous incoming stream of new fields to be observed and the number of fields with seven epochs shows that the strategy prevents an accumulation of fields not observed.

Table 1. Filter names, limiting magnitudes used to establish the exposure times and the corresponding exposures times, calculated using the exposure time calculator for bright nights. The "1exp" and "3exp" refer to the magnitude limits for an individual image and three combined images respectively. Mean and standard deviation estimated from the individual catalogues. J-VAR values are compared with those of J-PLUS DR1 (Cenarro et al. 2019) from coadded images. All values referred to $SNR > 5$ within a circular aperture of 3 arcsec.

Filter	m_{lim}^{1exp}	m_{lim}^{3exp}	t_{exp}	$\langle m_{lim}^{J-VAR} \rangle$	$\sigma_{m_{lim}}$	m_{lim}^{J-PLUS}
J0395	20.2	20.5	87	19.1	0.5	20.5
g	21.2	21.5	33	20.3	1.6	21.5
J0515	20.2	20.5	40	19.1	0.6	20.7
r	21.2	21.5	40	20.2	0.7	21.5
J0660	20.8	21.0	135	19.6	0.7	20.7
i	21.3	21.5	34	19.8	0.7	21.2
J0861	20.9	21.0	160	19.6	0.6	20.0

posure time calculator¹ and assume that the system will deliver observations 0.5-1 magnitudes shallower than the input value. The input limiting magnitudes and the exposure times for each band are shown in Table 1, together with actual average measures per filter from a sample of completed fields. As it can be seen, the individual exposures of J-VAR are between 0.4 (J0861) and 1.4 (J0395) magnitudes shallower than the stacked images of J-PLUS (in most of the cases, three images are combined). So it can be considered that the goal of the individual images of J-VAR being as deep as J-PLUS is overall fulfilled by the use of increased exposure times. It is worth noting that, in the case of J-PLUS, the observing exposure times are modulated according to the Moon phase and distance (Cenarro et al. 2019). This is possible because J-PLUS is carried out under photometric conditions. That approach was discarded for J-VAR both for simplicity, and

¹ <https://www.cefca.es/jplusetc/>

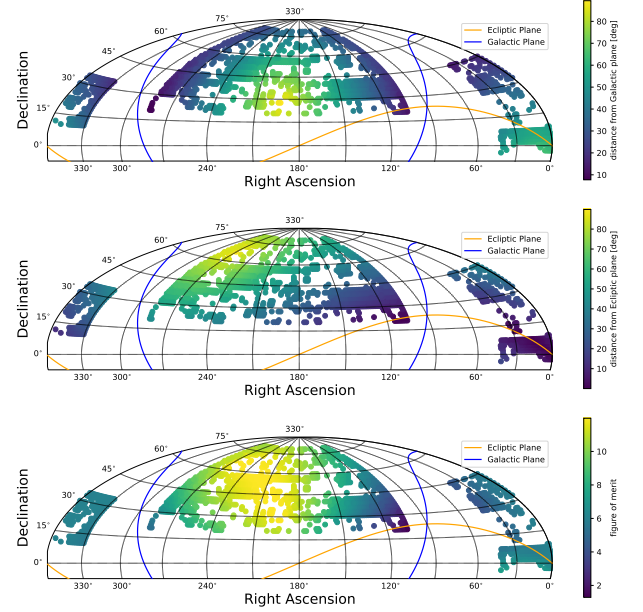


Fig. 3. The selection of the pointings to be observed is based on a trade off between the distance from the Galactic plane (top panel) and the distance from the Ecliptic plane (middle panel). The bottom panel shows the figure of merit given by the sum of the two previous panels (divided by 10 for convenience). At each right ascension, this provides the priority for the pointing to be observed.

because the survey is by construction carried out with varying atmospheric conditions that are difficult to track and model.

Regarding the selection of sky regions to be observed, two main considerations are taken into account. First, to ensure accurate photometric calibration, J-VAR targets J-PLUS fields that have already been published and properly calibrated. Second, the choice of fields is driven by the three key science cases of the survey: small bodies of the Solar System (Sect. 5.1), optical transients—particularly supernovae (Sect. 5.2), and variable stars (Sect. 5.3). The supernova case requires fields with a relatively low stellar density, which is best achieved by observing far from the Galactic plane. In contrast, the Solar System Objects case benefits from fields located as close as possible to the Galactic plane. This complementarity is illustrated in Fig. 3.

2.1.1. Time-domain design: cadence and observing sequence

Given the filler nature of the project, the cadence is primarily dictated by atmospheric conditions and the availability of other observing programs at any given time. The resulting cadence and sampling for J-VAR DR1 are shown in Fig. 4.

For supernovae, maximizing the time span of observations increases the likelihood of detecting events in different phases of their evolution. Therefore, a goal was set to span the campaign in each field for at least one year. Additionally, to facilitate the creation of template images from any observing epoch—defined as all observations taken within the same night—the basic observing block (BBO) was structured to consist of three exposures per filter across all seven bands. These triplets allow for stacking when needed, improving signal-to-noise and enabling high-quality template image generation. The exposures are not taken sequentially in the same band; instead, three full cycles through the seven filters are executed, distributing the observations in time. This strategy, illustrated in Fig. 5, ensures that each

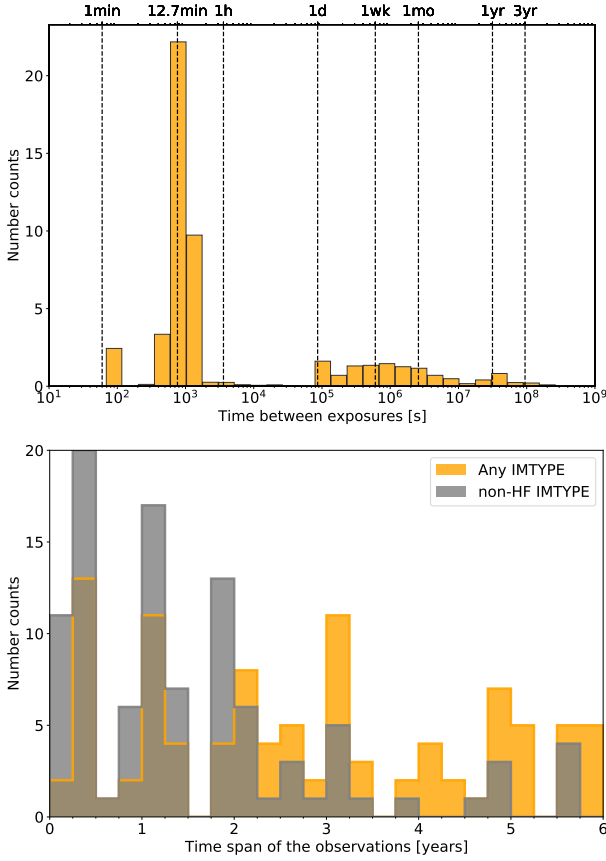


Fig. 4. Cadence and time span. *Top:* Histogram of the times between consecutive individual exposures in *g*-band along the observation of each field. The median of all fields is shown. The median time interval between exposures is 12.7 minutes. *Bottom:* Time span distribution of all J-VAR DR1 fields. In *gray*, nominal observations (JVN), while in *yellow*, any type of observation is shown (including also high-frequency observations).

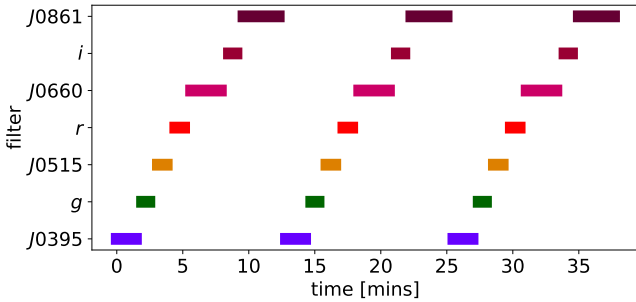


Fig. 5. Structure of an observing block. First an exposure in the seven filters is obtained, then a small dithering is applied, then a second sequence of exposures is executed and then a third one after a second dithering. The two dithering directions are orthogonal.

filter is sampled at different time intervals within an observing night. The full BBO takes approximately 40 minutes to complete, with a median gap of 12.7 minutes between exposures in the same filter.

This approach benefits not only the detection of transient events but also minor bodies in the Solar System, where repeated observations over short timescales help constrain orbital trajectories and facilitate rapid follow-up. Whenever possible, the same

field is observed on consecutive nights to improve trajectory predictions. On longer timescales, sampling on the scale of weeks is crucial for tracking the brightness evolution of supernovae. The final distribution of visit frequencies for a given field is illustrated in Fig. 4.

Beyond transients and Solar System objects, J-VAR was also designed to provide multi-band time-domain information for variable stars, with RR Lyrae stars serving as a reference case for defining the total number of epochs. Unlike transient detections, where the absolute timing of observations is critical, RR Lyrae characterization primarily depends on adequately sampling the pulsation cycle. Given the somewhat randomized observing cadence, this condition is generally fulfilled naturally over time.

To determine the optimal number of epochs required, a simulation was conducted using real RR Lyrae light curves from the OGLE III Catalog of Variable Stars (Soszyński et al. 2010, 2011) as a reference. The test focused on a single OGLE band (*I*), where different scenarios with varying numbers of randomly selected epochs were simulated. Each simulated epoch consisted of three data points, mirroring the J-VAR observing sequence. The derived periods were then compared to the true values provided by OGLE, allowing us to assess the period recovery success rate. The study found that at least 11 epochs were necessary to retrieve the correct period in $\sim 75\%$ of cases when using a single band and a signal-to-noise ratio (SNR) above 50. Given that J-VAR includes observations in seven filters, this success rate was expected to improve when considering multi-band data. Consequently, 11 epochs were adopted as a reasonable trade-off between ensuring period determination accuracy and maximizing the survey area. This choice is consistent with other surveys, such as Pan-STARRS (Sesar et al. 2017). The actual period recovery success rate for J-VAR DR1 is analyzed in the accompanying RR Lyrae catalogue paper (Kulkarni et al. submitted). Using only the J-VAR *r* band, *Gaia* DR3 (Gaia Collaboration et al. 2023; Clementini et al. 2023) periods of RR Lyrae stars in common are recovered within 1% relative difference in $\geq 70\%$ of the cases for *G* magnitude from 14 to 19. Some examples of J-VAR RR Lyrae light curves are shown in Sect. 5.3.

2.1.2. The High Frequency (HF) Fields

During periods around full Moon, one of the JAST80 filter wheels may be temporarily replaced to host alternative filters required by other projects (e.g. GALANTE, Maíz Apellániz et al. 2021). When atmospheric conditions prevent the execution of those programs, we implement a dedicated J-VAR observing strategy, hereafter the “high-frequency mode” (HF). In this mode, a single field is monitored continuously for ~ 3 hours, repeating the standard sequence of exposures with the set of available J-VAR filters J-VAR sequence of seven filters (Fig. 5). This configuration delivers intra-night light curves with much denser sampling than in the nominal survey, while maintaining full compatibility with the standard observing setup.

3. Data Reduction

The image reduction is performed using *jype*, a custom-built pipeline developed at the *Centro de Estudios de Física del Cosmos de Aragón* (CEFCA) for processing data from OAJ surveys (see, e.g. Cenarro et al. 2019; Bonoli et al. 2021). Written primarily in Python, *jype* incorporates SExtractor (Bertin & Arnouts 1996) for source extraction and initial photometry. The pipeline has been continuously developed since 2010, and its

most recent version before the release, `jype-3.1.9`, has been used for the processing of J-VAR DR1 images.

A key aspect of `jype` is its ability to handle the particular readout structure of the T80Cam CCD, which consists of 16 amplifiers. Each amplifier includes overscan and prescan regions along both the x and y axes, allowing for precise bias level removal. Immediately after observation, scientific images undergo an initial calibration using the latest valid flat field and illumination correction (see below). These pre-processed images are typically available within minutes and enable time-sensitive analyses, such as asteroid and transient detection, which are usually conducted the day after observation.

Beyond this real-time processing, a more refined reduction is performed at the end of each observing run, defined as a period during which the optical system remains stable (i.e., no interventions affecting the filter wheel or main mirror cleaning). Observing runs typically last about a month, at which point master flat fields and illumination corrections are generated to ensure optimal photometric accuracy.

In addition to standard image reduction steps, including bias subtraction, flat-fielding, fringing correction (when necessary), and cosmic ray and satellite trail masking, `jype` features an essential illumination correction step. This is particularly important for wide-field systems like JAST80, where conventional flat-fielding alone can introduce a two-dimensional photometric bias of several tens of millimagnitudes across the image due to the presence of field correctors. To mitigate this effect, an additional processing step is applied; see details in Appendix B.1 in Bonoli et al. (2021).

Finally, `jype` computes the aperture correction for photometry performed within a 6-arcsecond diameter integration area, which serves as a reference for total flux measurements in J-VAR DR1, particularly for point-like sources. This standardized photometric approach ensures consistency across all reduced data products.

4. First Data Release

The First Data Release of J-VAR was made public on 19th July 2024. The number of pointings distributed in this data release is 101, providing time-domain information for $\sim 202 \text{ deg}^2$ on the sky in seven photometric bands. The list of coordinates is in Table ??, together with information on the earliest and latest time of observation (in modified Julian date) and if the field has high frequency observations. In case HF observations are available, the earliest and latest time of observation is also available (again, as modified Julian date). The sky distribution is shown in Fig. 8. From an analysis of each of the images in this data release, we derived the distribution of limiting magnitudes (Fig. 6). The limiting magnitudes are rarely achieved in most filters and never achieved in the reddest filters (*J0861* and *i*). This is a consequence of the approximations made at the time of setting the exposure times. Similarly, Fig. 7 shows the distribution of the FWHM. The lower limit of the distribution is close to 1 arcsec which is slightly smaller than 2 pixels. The peak of the distribution is consistently close to 1.5 arcsec. The quality of the data, in particular having a shallower survey in the red, does not affect the main goals of the project, as the multi-filter light curves are still deliverable.

The data of J-VAR DR1 are accessible through the CEFCA archive². The principal way to access to the data is through the

public catalogue, whose structure is related to the main objectives of the project. The time of observation of each field in a given filter is in the `Timestamps` table (its contents are shown in Table B.3). In this table, the observing time of each image is provided. Each image is identifiable via the identifier of the field and the identifier of the filter. The time is provided as coordinated universal time (UTC). For convenience, the modified Julian date (MJD) is also given.

Each image is also tagged according to the type of observation: regular or high frequency (see above). The regular J-VAR observations are tagged as “JVN”. The high frequency observations are marked differently, as described hereafter. The narrow-band images are marked as “HFN”. The broad-band images are marked “HFF” if executed with the same filters as the main “JVN” survey. If they are acquired using, not the same physical filters, but the g , r , and i filters initially devoted to the Pathfinder camera to conduct of the miniJPAS survey (Bonoli et al. 2021), they are named “HFG”. Those gri filters were usually mounted in the auxiliary filter wheel of T80Cam, and were manufactured following the same optical design.

The photometry of each object is provided in the `Photometry` table (a description is made available in Table B.4). In this table, each observation of an object is identified by an ID of the object. Both the J-PLUS identifier (the ID of the J-PLUS DR3 tile and the identifier of the object within the tile) and the J-VAR identifier (the string `jvar` followed by the right ascension and the declination of the object) are provided. The magnitudes and associated errors are offered as arrays. The full-width at half maximum of the objects is also provided as array, as well as a list of photometric flags which can be used for quality assessment. Finally, the photometric calibration is represented by an array containing the values used to go from instrumental magnitude to calibrated magnitude. The number of comparison stars and the maximum radius within which these stars are located are also shown. For details, see Pyrzas et al. (submitted). For convenience, the previous two tables are combined in a `light_curves` table whose columns are described in Table B.2.

The table `Objects` conveniently gathers useful information from J-PLUS DR3 (magnitudes in 3 and 6 arcsec, different star/galaxy separation indicators, FWHM), the interstellar extinction, the type and period of variability according to the International Variable Stars Index and the parallax, G magnitude, variability class and score from Gaia DR3. The columns of this table are summarised in Tab.B.

Two tables related to the Solar System Objects are also available. The first one (`SSOs_DETECTIONS`, the columns are shown in Table B.5) shows the detections by the SSOS pipeline, described in Sect. 5.1 and in Morate et al. (submitted), while the second one (`SSOs_MAGNITUDES`, whose columns are shown in Table B.6) shows the magnitudes for each object.

Following the common practice, the detections of optical transients are reported through the Transient Name Service³ and therefore there is no associated table in the database.

All the tables are accessible via a web interface and via the Table Access Protocol of the Virtual Observatory, both in a programmatic way (e.g. with Python) or via programs like TOPCAT (Taylor 2005). Similarly, The reduced images are accessible through the archive and through the Simple Image Access Protocol (SIAP) of the Virtual Observatory. An example of how to access the data of J-VAR is available at https://github.com/aederoc1/J-VAR_paper1.

² <https://archive.cefca.es/catalogues/jvar-dr1>

³ <https://www.wis-tns.org/search>

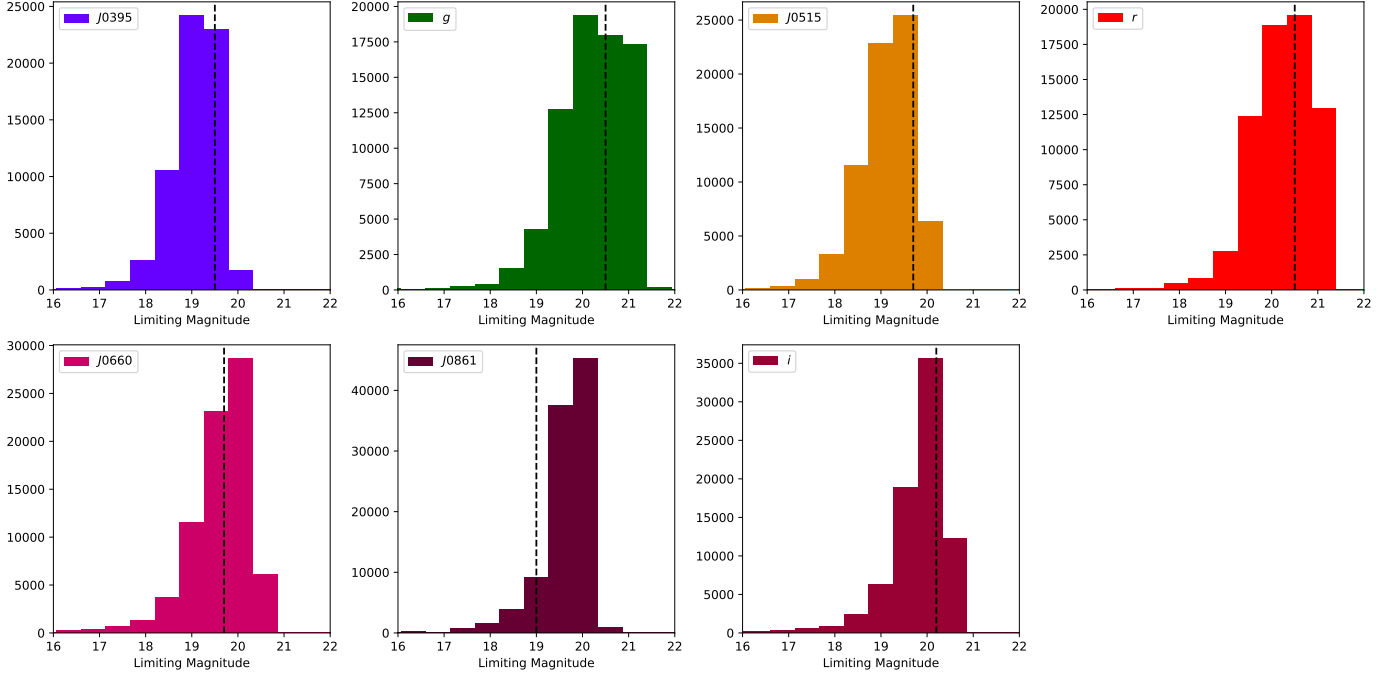


Fig. 6. Distribution of the limiting magnitudes of all the images of J-VAR DR1 in the different filters. The vertical line is one magnitude shallower than J-PLUS limiting magnitude (5σ detection in 6 arcseconds aperture) which was used to define the exposure times of J-VAR.

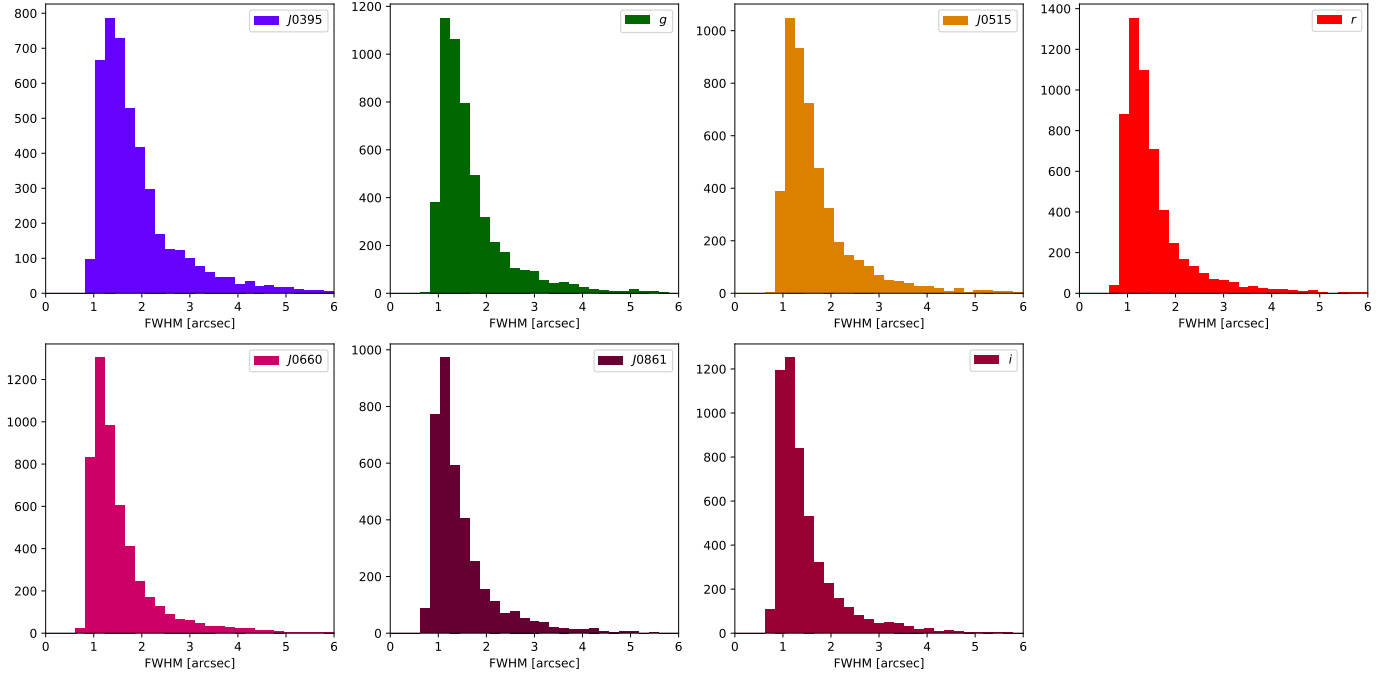


Fig. 7. Distribution of the median full width at half maximum of the detected sources in each image for each observed filter. The quasi-simultaneous observations in the different filters and the good image quality across the whole optical range result in very similar distributions, regardless of the central wavelength of the filter.

5. Science Cases

5.1. Small bodies of the Solar System

Small bodies (SB) in the Solar System are not usually the drivers of observational surveys, with the noticeable exceptions of the Asteroid Terrestrial-impact Last Alert System, ATLAS, (Tonry et al. 2018), the Panoramic Survey Telescope and Rapid Re-

sponse System, PAN-STARRS (Hodapp et al. 2004), or the Rubin Observatory's Legacy Survey for Space and Time, LSST (Ivezić et al. 2019b) surveys. SBs are usually regarded as contamination for the main science objectives of most large surveys. Nevertheless, the SB community has exploited this "contamination" by developing pipelines that detect and extract their information. The Sloan Digital Sky Survey has been largely exploited for SB (e.g., Ivezić et al. 2001; DeMeo & Carry 2013) and so was

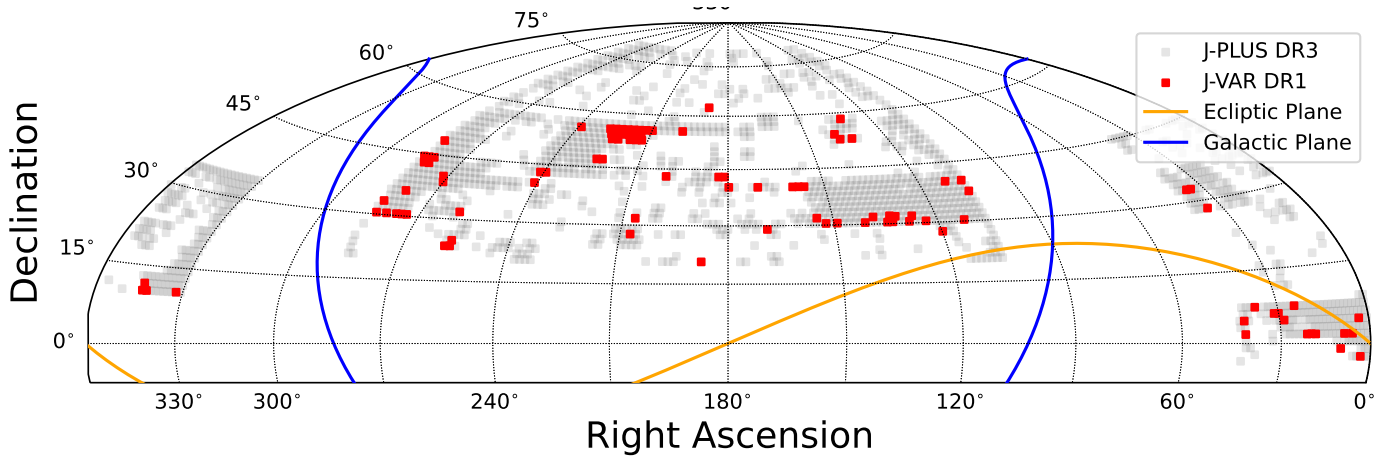


Fig. 8. The red markers show the sky distribution of the 101 pointings of J-VAR DR1. The grey points refer to the sky distribution of J-PLUS DR3 which is used for calibration. The yellow and the blue line show the Ecliptic and the Galactic plane, respectively.

the first data release of J-PLUS (see Morate et al. 2021). Sykes et al. (2000), Popescu et al. (2016) and Mahlke et al. (2018) have extended this search to infrared wavelengths. SBs information, such as their colors, is used for mineralogical analysis, which places strong constraints on how different materials are distributed in the Solar System and, together with dynamical and collisional models, may shed light into how the Solar System as we know it today came to be.

J-VAR observational strategy is well-suited for the detection of SBs because the fields (Sect. 2.1) are selected as a balance between its three main science drivers. Within the 101 fields included in J-VAR DR1, there are 131 900 individual detections, i.e., an asteroid was detected in one of the J-VAR filters. These detections correspond to a total of 6 570 individual asteroids, some of them detected in two or more epochs.

The detection of the SBs is done using the SOSS pipeline (see details in Mahlke et al. 2019). The pipeline detects and extracts the instrumental magnitude of the SBs, but it does not produce calibrated magnitudes because the J-VAR data is taken during non-photometric nights. Thus, no zero points are provided in the images' headers. Therefore, the calibration step is done using J-PLUS observed fields, computing the zero points for the common objects in the field and applying this secondary calibration to the SB (more details are provided in Morate et al. submitted).

Regarding the number of detections, for those J-VAR fields centered around the ecliptic plane of the Solar System (± 10 deg), there are around ~ 400 detections per epoch (which translates roughly into ~ 30 different objects). This number decreases as one moves away from the ecliptic: for high latitudes, i.e., above 30 deg, the number of detections is very scarce, usually below 20 (this is, one object or none at all.) However, the number of detected objects ensures good statistics (see below).

The distribution of objects observed with a given number of filters peaks at six (with about 3 000). Almost 800 were observed with all seven filters, and only two objects were observed with one filter. We show the number of detections per filter in Fig. 9. The lower numbers in the *J0395* and *J0515* filters were expected as these are narrow-band filters, and, in the case of the *J0395* filter, the reflectance of SB is known to decrease significantly at blue wavelengths. The most efficient filters are the SDSS filters *g*, *r*, and *i*, which was expected because these are the widest filters in the J-VAR system.

Finally, we show a highlight of our results (a detailed description of the data is provided in Morate et al., submitted):

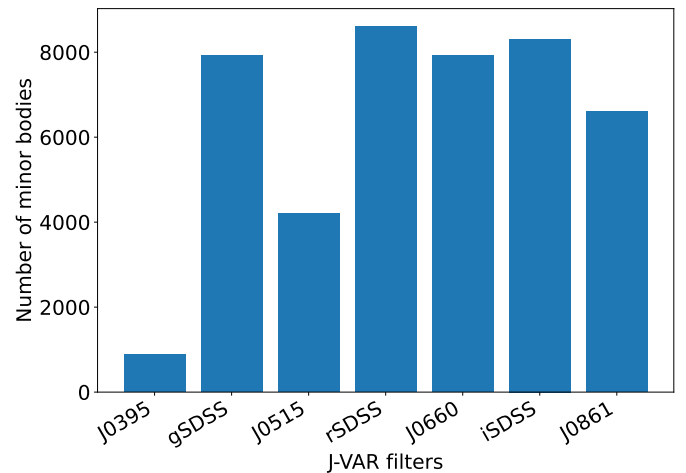


Fig. 9. Number of SBs detected in each J-VAR filter.

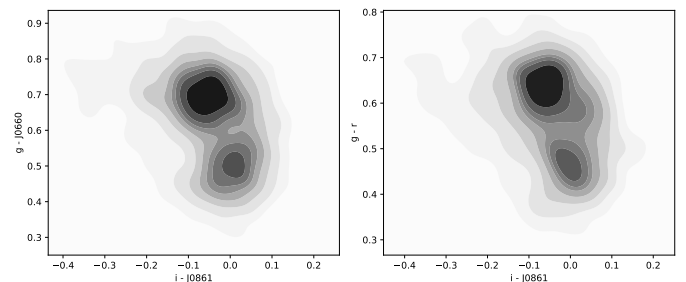


Fig. 10. Colour-colour diagram in the form of heat maps. The left panel shows $g - J0660$ vs $i - J0861$, while the right panel shows $g - r$ vs $i - J0861$. The use of different colours allows to separate between families of different chemical composition.

Fig. 10 shows two colour-colour diagrams, zoomed into their densest regions to avoid outliers.

In Morate et al. (submitted) we present a value added catalogue (VAC) for J-VAR's DR1: the detection catalogue with calibrated magnitudes, RA, DEC, time of observation, among other useful information. We also provide a first look into the taxonomy of the objects and rotational properties of some targets, mostly observed in HF fields. In conclusion, J-VAR works

as a stand-alone survey, but, importantly, it nicely complements J-PLUS, which uses all J-VAR filters.

5.2. Optical Transients

Ranging from novae, supernovae (SNe) up to the progenitors of the most powerful gravitational waves, the transient sky is part of the most challenging puzzles in astrophysics and cosmology. Although mostly known as responsible for the first evidences of the Dark Energy dominated Universe in the late 1990s, type Ia SNe, for example, are still of paramount importance to cosmology. The so-called "Hubble tension" (Knox & Millea 2020), a discrepancy in the measurement of the Hubble constant in different stages of the Universe's evolution, is becoming a decade-long problem and some of the most precise results on which it relies are based on observations of low-redshift type Ia SNe.

From an astrophysical point of view, there seems to be still no universal consensus on the nature of type Ia SNe progenitors and their explosion mechanisms (Liu et al. 2023). The same difficulties arise in finding a single model to explain superluminous SNe explosions (Gal-Yam 2019).

As commented in Sect. 1, a variety of surveys aim at the study of the transient sky. In particular, currently ASAS-SN and ZTF which can be considered a progenitor of LSST.

We took advantage of the repeated visits from J-VAR and applied the image subtraction or differential image technique to look for optical transients within DR1 images. Our differential image pipeline consists in a sequence of open source packages and scripts to perform image subtraction and produce a catalogue of candidates to be analysed individually. The pipeline, optimized for SNe detection, also recovers variable stars, AGN, and asteroids. To reduce false positives, we apply strict shape and multi-band detection criteria, followed by SIMBAD cross-matching. The final step is a visual inspection and confirmation of the candidates.

Since our search was performed after the observations of a given field were completed, the pipeline detected some candidates which had been already observed by other surveys, which is the case for supernovae SN 2017icq (SN Ia), SN 2019obw (SN Ia), SN 2020cvy (SN II) and SN 2020amv (SN II) and transient candidates AT 2017eke, AT 2017dzn, AT 2018fds, AT 2019roh, AT 2019ioo and AT 2020abzu. Fig. 11 shows the detection, light curve and spectral energy evolution of the supernova SN 2020amv⁴. This was discovered on 23rd January 2020 and it is detected in J-VAR field 13 days after discovery. The bottom panel of Fig. 11 shows an excess in the J0660 filter, suggesting the presence of H α in emission, characteristic of type II supernovae, thus showing the potential of J-VAR to characterise low-redshift supernovae without the need of spectroscopy.

Our final lists of transient candidates contained a large number of variable sources. We recorded 252 known variable stars and 50 known AGN, along with 236 variable star candidates and 18 AGN candidates.

Finally, we have discovered by visual inspection four transient events which were submitted to the TNS database. Two of them, SN 2020admb (JVAR20a) and SN 2024slh (JVAR24b), were successively confirmed as supernovae and classified by the ZTF collaboration as a type Ia supernovae at redshifts 0.04 and 0.05, respectively. The other two, AT 2021aggy (JVAR21a) and AT 2024bxn (JVAR24a) are still classified as transient candidates at the TNS database.

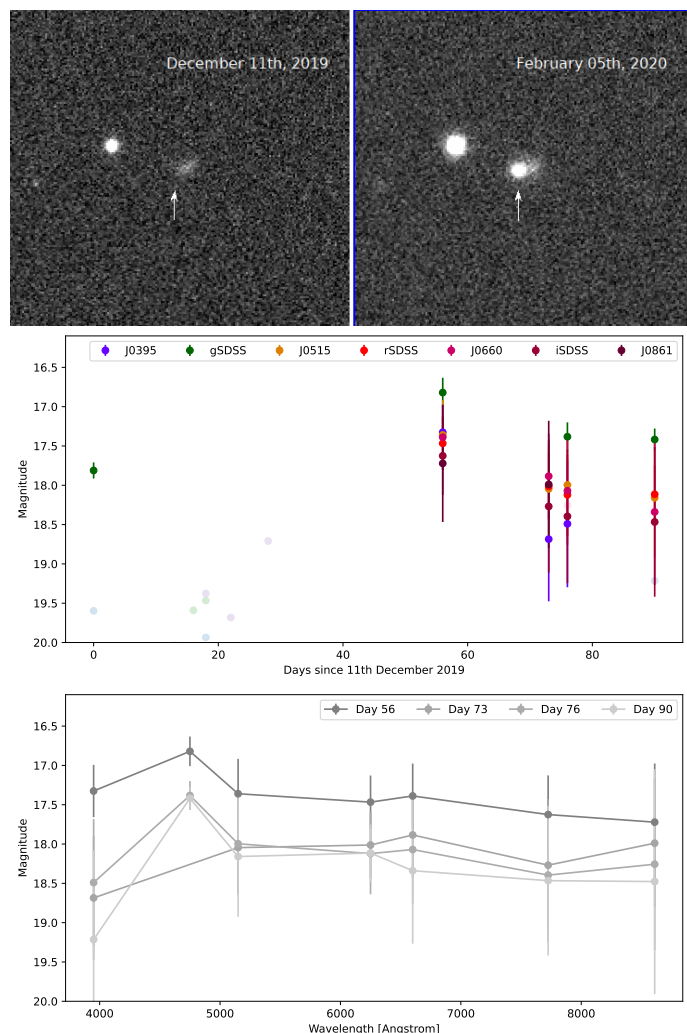


Fig. 11. *Top:* Detection image of SN 2020amv, *Middle:* Light curve of SN 2020amv in the seven filters of J-VAR. The shaded points refer to photometric errors larger than 1 magnitude, which is equivalent to a non detection. *Bottom:* Evolution of the spectral energy distribution of SN 2020amv with time. Note the detection of flux in the J0660 filter, confirming the nature of the object as a type II supernova.

5.3. Variable Stars

The J-VAR survey provides multi-band time-domain data that enables the study of various classes of variable stars across a range of timescales, amplitudes, and wavelengths. The combination of its multi-filter approach, flexible cadence, and moderate number of epochs makes it particularly well-suited for the characterization of pulsating stars, close or contact eclipsing binaries, and semi-regular variables. Moreover, the irregular spacing of the epochs mitigates aliasing effects in period determination, thereby increasing the robustness of variability classification.

The light curves for all the point-sources in common with J-PLUS have been extracted. This sums up to 1.3 million sources. The light curves have been obtained with ensemble differential photometry (see e.g., Everett & Howell 2001; Tamuz et al. 2005). For each star, at least 15 comparison stars are selected. In all cases, this is achieved in a search radius smaller than 9 arcminutes. The resulting photometric precision (RMS) is 2% down to mag ~ 16 and 5% to mag ~ 18 in the broad-band filters. The extraction and calibration process is described in detail in Pyrzas et al. (submitted). In total, the J-VAR DR1 catalogue has

⁴ <https://www.wis-tns.org/object/2020amv>

Table 2. Number of most occurring stellar objects (i.e. does not consider AGNs) in Objects table based on *Gaia* DR3 variability classes.

object	number	
SOLAR_LIKE	Solar-like variability	4176
ECL	Eclipsing binaries	1165
RS	RS Canum Venaticorum	1033
DSCT GDOR SXPH	δ Scuti / γ Doradus/ SX	901
	Phoenixis stars	
S	Short-timescale	494
LPV	Long-period variables	286
RR	RR Lyrae stars	315

1621 objects classified as variables in VSX and 15221 objects classified as variables in *Gaia* DR3. The most frequent stellar *Gaia* DR3 classes are shown in Table 2.

The variety of stellar systems that show changes in luminosity is very rich (e.g. Catelan & Smith 2015). The Hertzsprung-Russell diagram in Fig. 12 shows the locations of the objects whose light curves are shown in Fig. 13. The effective cadence of the observations favours the suitability of the study of some type of variable stars over others. In particular it fits well to the variability time-scales of RR Lyrae stars, Cepheids, high-amplitude δ Sct stars, semi-detached or contact binaries (with short or no interruptions between eclipses), etc. Conversely, the phase coverage is often not good for detached binaries because their eclipses last for a relatively short time in comparison with the whole period, so the probability of capturing both adequately is relatively low. And lastly, long-period variable stars, with periods of hundreds of days, are usually covered by the temporal baseline of J-VAR that typically extends beyond 1 year, although the phase is more irregularly sampled in this case than for shorter period variables mentioned before.

5.3.1. Pulsating stars: RR Lyrae, Cepheids, and δ Scuti stars

RR Lyrae stars were a key reference in defining the J-VAR cadence and total number of epochs, as they serve as excellent standard candles for distance determination in the Milky Way and nearby galaxies. The survey’s seven-band photometry allows for refined period determinations, variability classification, and potential metallicity estimates based on color indices. The adopted 11-epoch strategy ensures that light curves sample the pulsation cycle adequately, improving period recovery rates compared to single-band surveys.

In addition to RR Lyrae stars, J-VAR data can also be used to identify and study classical Cepheids and δ Scuti stars, which provide complementary constraints on stellar evolution and pulsation theory. Given that J-VAR primarily targets the Galactic halo, the survey contains only a small number of Cepheids. The multi-band nature of the survey is particularly useful for distinguishing between different pulsation modes and for improving period-luminosity relationships.

5.3.2. Eclipsing binaries and other periodic variables

The survey’s multi-epoch observations facilitates the identification and classification of semi-detached (EB) and contact (EW) eclipsing binaries, and in fewer cases, detached (EA) systems. The broad wavelength coverage helps to constrain better the temperature ratios between the components (e.g. Kallrath & Milone 2009), improving constraints on stellar parameters. Additionally, J-VAR’s ability to capture multiple points within an eclipse event

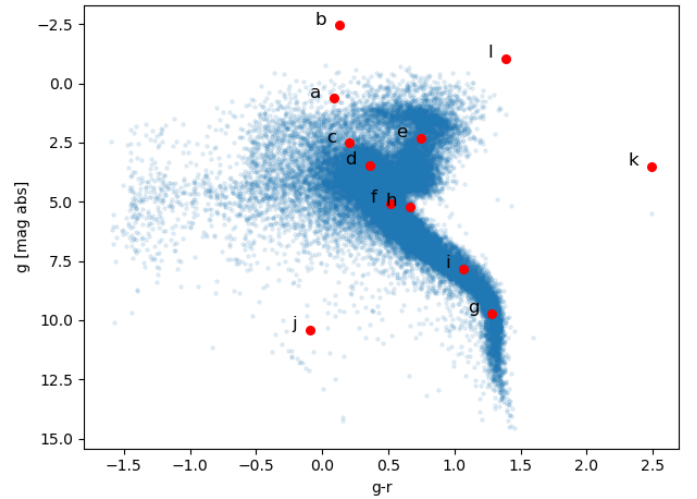


Fig. 12. The colour-magnitude diagram of J-VAR sources. The light curves of the objects marked in red are shown in Fig.13.

in a single observing block increases its potential for detecting and characterizing short-period systems.

Other periodic variables, such as rotationally modulated stars, including RS CVn (RS), chromospherically active rotational binaries, and BY Dra (BY), late-type dwarf stars with starspots and rotational modulation, can also be analysed using J-VAR data. The survey’s multi-band information helps distinguish between RS and BY stars.

5.3.3. Semi-regular and cataclysmic variables

The J-VAR cadence also enables the detection of longer-term variations associated with semi-regular and Mira variables, which exhibit large-amplitude, multi-periodic brightness fluctuations. Additionally, the survey’s transient monitoring capabilities may allow for serendipitous detections of eruptive variables, including cataclysmic variables (CVs) undergoing outbursts.

The presence of short intra-night separations in the observing strategy further provides sensitivity to flickering behaviour in CVs and rapidly variable phenomena in compact stellar remnants. Combined with spectroscopic follow-up, these data could contribute to the discovery of rare or previously unknown subclasses of variable stars.

6. Conclusions and perspectives

The parameter space for time-domain wide-field photometric surveys can be summarized by six factors: (i) survey area – the amount of sky area where the light curves are distributed, (ii) cadence – the time interval between two observations of the same targets, (iii) limiting magnitude, (iv) number of filters used to characterize a light curve, (v) pixel scale of the camera, and (vi) field of view⁵. The science cases driving the different projects are reflected in how they cover such parameter space (see Fig. 14). Since TESS is aiming at transits of extrasolar planets, its cadence is very short with respect to all other projects. TESS also employs a vast field of view and a very large pixel scale. With

⁵ In this analysis we are not using the etendue (the multiplication of the size of the primary mirror by the field of view) or the exposure time, since they are somewhat embedded in the values that we are considering, in particular limiting magnitude and cadence

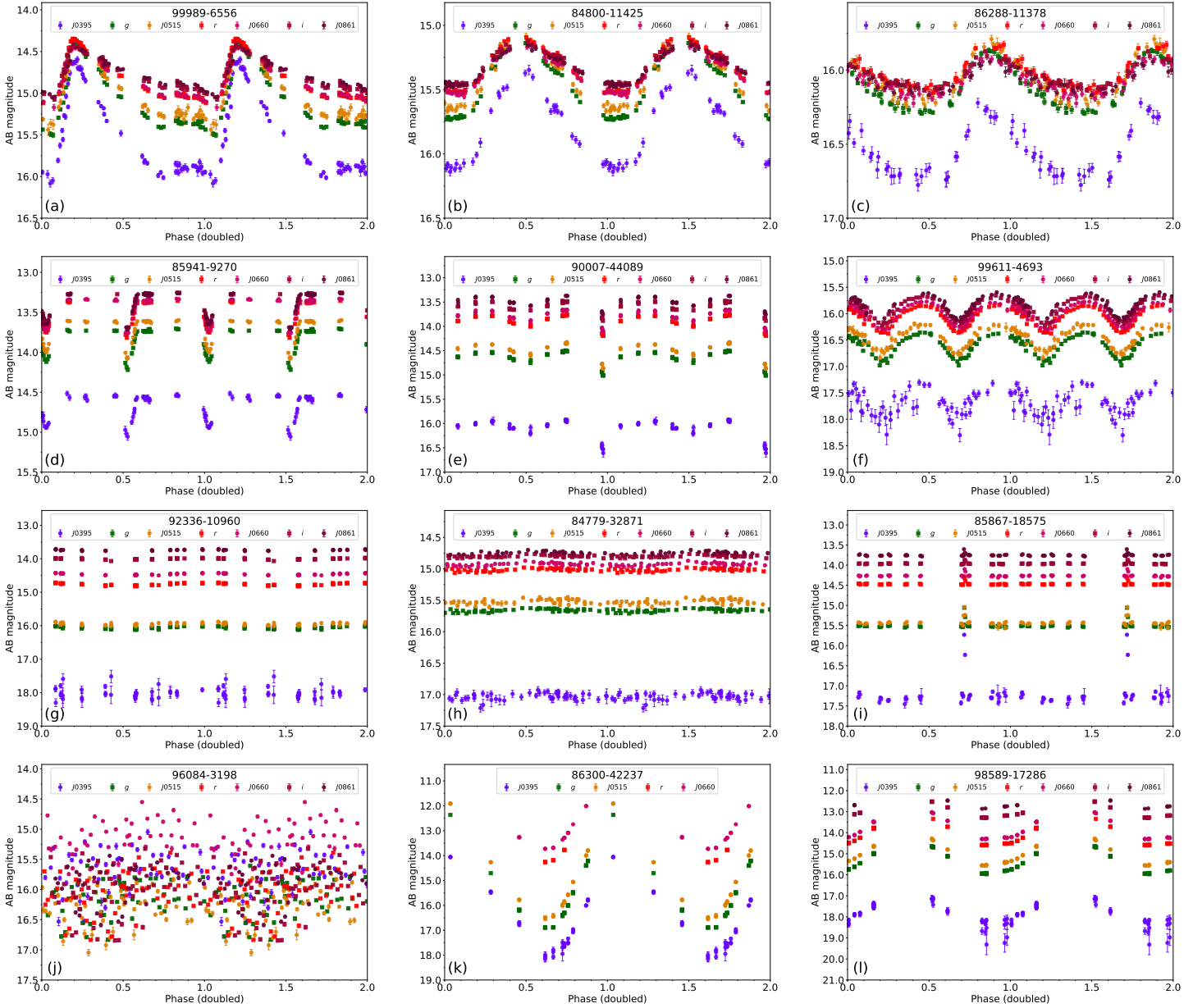


Fig. 13. Phase-folded light curves of variable stars from J-VAR DR1 with known periods, P . Periods are taken either from Kulkarni et al. (submitted, \star) or from VSX (Watson et al. 2022; \dagger). The phase has been duplicated to clearly show the full brightness variation cycle. *From top-left to bottom-right:* (a) RRab ($P^\star = 0.55630$ d), (b) RRC ($P^\star = 0.38300$ d), (c) high-amplitude δ Scuti pulsating stars ($P^\dagger = 0.04862$ d), (d) EA ($P^\dagger = 1.17814$ d), (e) EB ($P^\dagger = 8.98140$ d), and (f) EW ($P^\dagger = 0.28265$ d) eclipsing binaries, (g) BY Dra ($P^\dagger = 8.67666$ d), (h) RS CVn ($P^\dagger = 0.17216$ d), (i) RS CVn with a possible flare ($P^\dagger = 1.64620$ d), (j) CV ($P^\dagger = 0.06799$ d), (k) LPV M ($P^\dagger = 262.31$ d), and (l) SR ($P^\dagger = 143.00$ d) variables. The OBJ_IDs are shown in each panel. Light curve generation is described in Pyrzas et al. (submitted).

the noticeable exception of ZTF, ground based projects have all comparable fields of view and pixel scales. This is mostly due to the need of having an optical system which is adapted to the atmospheric conditions of the observing site. The three parameters where there is the largest scatter are sky area, limiting magnitude, and number of filters. Ground-based transient surveys like ZTF and ASAS-SN cover a very large sky area in a small number of filters as often as possible. The main difference between these two surveys is the limiting magnitude (ZTF is carried out with a larger telescope) and the survey area (ZTF is carried out with one telescope only, thus only covering the Northern celestial hemisphere, while ASAS-SN, being a network of telescopes, can survey the whole sky). The observing strategy of LSST is the result of the trade off between different projects, which makes

the number of filters larger than other surveys and the cadence somewhat less frequent, although it has an unrivalled depth.

J-VAR leverages three characteristics of the JAST80 telescope: good image quality, wide field of view, and the narrow band filters. To the best of our knowledge, at the time of beginning the survey (2017), J-VAR was the only wide-field time-domain survey routinely observing with narrow-band filters. This brings J-VAR to occupy a unique position in the phase-space for wide-field time-domain surveys as the cadence is comparable with the one of LSST, the depth comparable with ZTF, and the filter set is unique.

J-VAR is not carried out with a dedicated telescope, unlike other time-domain surveys, and therefore shares observing time with other awarded proposals. Projects like ASAS-SN and ZTF

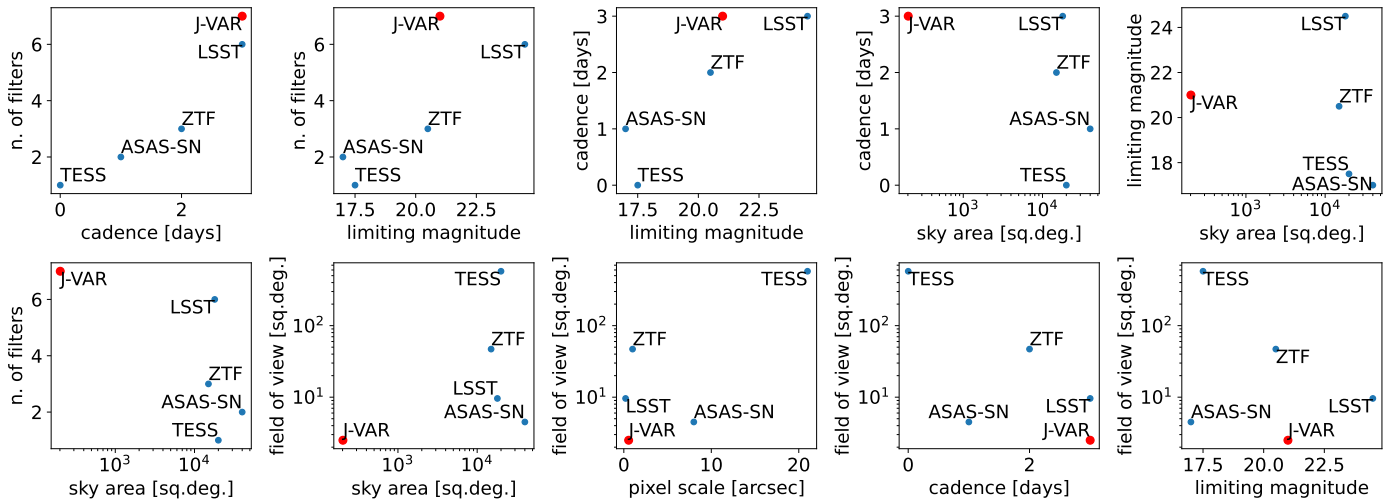


Fig. 14. Scatter plots comparing the main characteristics of J-VAR DR1 (highlighted in red) with respect to other wide-field photometric surveys.

can observe within a few days all the sky available from their sites and, therefore, they can, in principle, be extended indefinitely to increase the length of the light curves. In the case of J-VAR, the observation of a field is limited to 11 epochs. The number of completed fields grows at a rate of approximately 58 square degrees per year (see Fig 2). This has been roughly constant since the beginning, when J-VAR was carried out as a two-years long large project at the OAJ, and now when it is a filler among J-PLUS and the Legacy Surveys at the OAJ. It is likely that J-VAR will continue at the same pace until 2027, when the Legacy Surveys will end. At the current rate, J-VAR will reach 1000 square degrees in 2035, although this could vary in case of changes in the programs carried out on the JAST80 after 2027.

Adopting a unique strategy leveraging narrow band filters, J-VAR represents an unprecedented opportunity for time-domain astrophysics. Thanks to the use of narrow-band filters, J-VAR constitutes a bridge between spectroscopic time-domain surveys (e.g., SDSS-V; Kollmeier et al. 2025) and wide-field photometric surveys. J-VAR’s cadence and wavelength coverage make it complementary to large-scale surveys such as *Gaia*, ZTF, and LSST. While those surveys provide extensive temporal coverage, J-VAR adds the advantage of quasi simultaneous multi-band observations, aiding in precise classification and improving constraints on variability mechanisms. The multi-filter approach also facilitates cross-matching with existing variability catalogues, enabling further refinement of classification schemes. The high-frequency mode further extends J-VAR’s scope, enabling intra-night variability studies (asteroids, eclipsing binaries, CVs) not accessible in most wide-field surveys.

J-VAR DR1 contains 1.3 million light curves of 11 epochs in seven photometric bands with no selection bias on colour or type. By covering a diverse range of variable star types, J-VAR provides a unique dataset for time-domain astrophysics. The combination of multiple bands, strategically spaced epochs, and intra-night sampling opens the door to numerous scientific applications, from refining period-luminosity relations to characterizing new classes of variables. The survey’s contribution to variable star studies will be further enhanced through future data releases and dedicated variability catalogues, ensuring an average of 5000 new multi-band light curves per newly observed square degree.

Acknowledgements. We acknowledge support from the Governments of Spain and Aragón through their general budgets and the Fondo de Inversiones de Teruel. The Spanish Ministry of Science and Innovation (MCIN/AEI/10.13039/501100011033) and ERDF, A way of making Europe with grant PID2021-124918NB-C42. AE acknowledges the financial support from the Spanish Ministry of Science and Innovation and the European Union - NextGenerationEU through the Recovery and Resilience Facility project ICTS-MRR-2021-03-CEFCA. DM acknowledges the financial support from the European Union - NextGenerationEU through the Recovery and Resilience Facility program Planes Complementarios con las CCAA de Astrofísica y Física de Altas Energías - LA4. SK has received financial support from the Aragonese Government through the Research Groups E16_23R and the Spanish Ministry of Science and Innovation (MCIN/AEI/10.13039/501100011033 y FEDER, Una manera de hacer Europa) with grant PID2021-124918NB-C41. AAC acknowledges financial support from the Severo Ochoa grant CEX2021-001131-S funded by MCIN/AEI/10.13039/501100011033. AAC and DM acknowledge financial support from the Spanish project PID2023-153123NB-I00, funded by MCIN/AEI. P.C. acknowledges financial support from the Spanish Virtual Observatory project funded by the Spanish Ministry of Science and Innovation/State Agency of Research MCIN/AEI/10.13039/501100011033 through grant PID2023-146210NB-I00. F.R.H. acknowledges support from FAPESP grants 2018/21661-9 and 2021/11345-5. The authors would like to acknowledge the use of the following open-source software packages that were essential in the analysis presented herein: Python, NumPy, Astropy, pandas, matplotlib, and PyVO (including TAP). Their combined functionality enabled efficient data handling, manipulation, visualization, and access to Virtual Observatory services.

References

- Auvergne, M., Bodin, P., Boissard, L., et al. 2009, *A&A*, 506, 411
- Bellm, E. C., Kulkarni, S. R., Graham, M. J., et al. 2019, *PASP*, 131, 018002
- Benítez, N., Dupke, R., Moles, M., et al. 2014, *arXiv e-prints*, arXiv:1403.5237
- Bertin, E. & Arnouts, S. 1996, *A&AS*, 117, 393
- Bonoli, S., Marín-Franch, A., Varela, J., et al. 2021, *A&A*, 653, A31
- Borucki, W. J., Koch, D., Basri, G., et al. 2010, *Science*, 327, 977
- Catelan, M. & Smith, H. A. 2015, *Pulsating stars* (John Wiley & Sons)
- Cenarro, A. J., Moles, M., Cristóbal-Hornillos, D., et al. 2019, *A&A*, 622, A176
- Cenarro, A. J., Moles, M., Marín-Franch, A., et al. 2014, in *Society of Photo-Optical Instrumentation Engineers (SPIE) Conference Series*, Vol. 9149, *Observatory Operations: Strategies, Processes, and Systems V*, ed. A. B. Peck, C. R. Benn, & R. L. Seaman, 914911
- Clementini, G., Ripepi, V., Garofalo, A., et al. 2023, *A&A*, 674, A18
- del Pino, A., López-Sanjuan, C., Hernán-Caballero, A., et al. 2024, *A&A*, 691, A221
- DeMeo, F. E. & Carry, B. 2013, *Icarus*, 226, 723
- Drake, A. J., Djorgovski, S. G., Mahabal, A., et al. 2009, *ApJ*, 696, 870
- Everett, M. E. & Howell, S. B. 2001, *PASP*, 113, 1428
- Gaia Collaboration, Vallenari, A., Brown, A. G. A., et al. 2023, *A&A*, 674, A1
- Gal-Yam, A. 2019, *Annual Review of Astronomy and Astrophysics*, 57, 305
- Hodapp, K. W., Kaiser, N., Aussel, H., et al. 2004, *Astronomische Nachrichten*, 325, 636
- Hubble, E. 1929, *PNAS*, 15, 168

- Ivezić, Ž., Kahn, S. M., Tyson, J. A., et al. 2019a, *ApJ*, 873, 111
- Ivezić, Ž., Kahn, S. M., Tyson, J. A., et al. 2019b, *ApJ*, 873, 111
- Ivezić, Ž., Tabachnik, S., Rafikov, R., et al. 2001, *AJ*, 122, 2749
- Kallrath, J. & Milone, E. F. 2009, *Eclipsing Binary Stars: Modeling and Analysis*, 2nd edn. (New York: Springer-Verlag)
- Knox, L. & Millea, M. 2020, *Phys. Rev. D*, 101, 043533
- Kollmeier, J. A., Rix, H.-W., Aerts, C., et al. 2025, *arXiv e-prints*, arXiv:2507.06989
- Leavitt, H. S. & Pickering, E. C. 1912, "Harvard College Observatory Circular", 173, 1
- Liu, Z.-W., Röpke, F. K., & Han, Z. 2023, *Research in Astronomy and Astrophysics*, 23, 082001
- López-Sanjuan, C., Vázquez Ramió, H., Varela, J., et al. 2019, *A&A*, 622, A177
- López-Sanjuan, C., Vázquez Ramió, H., Xiao, K., et al. 2024, *A&A*, 683, A29
- Mahlke, M., Bouy, H., Altieri, B., et al. 2018, *A&A*, 610, A21
- Mahlke, M., Solano, E., Bouy, H., et al. 2019, *Astronomy and Computing*, 28, 100289
- Maíz Apellániz, J., Alfaro, E. J., Barbá, R. H., et al. 2021, *MNRAS*, 506, 3138
- Marín-Franch, A., Taylor, K., Cenarro, J., Cristobal-Hornillos, D., & Moles, M. 2015, in *IAU General Assembly*, Vol. 29, 2257381
- Marín-Franch, A., Taylor, K., Cepa, J., et al. 2012, in *Society of Photo-Optical Instrumentation Engineers (SPIE) Conference Series*, Vol. 8446, Ground-based and Airborne Instrumentation for Astronomy IV, ed. I. S. McLean, S. K. Ramsay, & H. Takami, 84466H
- Mayor, M. & Queloz, D. 1995, *Nature*, 378, 355
- Morate, D., Marcio Carvano, J., Alvarez-Candal, A., et al. 2021, *A&A*, 655, A47
- Oke, J. B. & Gunn, J. E. 1983, *ApJ*, 266, 713
- Popescu, M., Licandro, J., Morate, D., et al. 2016, *A&A*, 591, A115
- Ricker, G. R., Winn, J. N., Vanderspek, R., et al. 2015, *Journal of Astronomical Telescopes, Instruments, and Systems*, 1, 014003
- Sesar, B., Hernitschek, N., Mitrović, S., et al. 2017, *AJ*, 153, 204
- Shappee, B. J., Prieto, J. L., Grupe, D., et al. 2014, *ApJ*, 788, 48
- Soszyński, I., Dziembowski, W. A., Udalski, A., et al. 2011, *Acta Astron.*, 61, 1
- Soszyński, I., Udalski, A., Szymański, M. K., et al. 2010, *Acta Astron.*, 60, 165
- Sykes, M. V., Cutri, R. M., Fowler, J. W., et al. 2000, *Icarus*, 146, 161
- Tamuz, O., Mazeh, T., & Zucker, S. 2005, *MNRAS*, 356, 1466
- Taylor, M. B. 2005, in *Astronomical Society of the Pacific Conference Series*, Vol. 347, *Astronomical Data Analysis Software and Systems XIV*, ed. P. Shopbell, M. Britton, & R. Ebert, 29
- Tonry, J. L., Denneau, L., Heinze, A. N., et al. 2018, *PASP*, 130, 064505
- Watson, C., Henden, A. A., & Price, A. 2022, *VizieR Online Data Catalog: AAVSO International Variable Star Index VSX (Watson+, 2006-)*, *VizieR On-line Data Catalog: B/vsx*. Originally published in: 2006SASS...25...47W

Appendix A: Pointings in J-VAR DR1

The coordinates of the pointings of J-PLUS DR1 are shown in Table ???. These are the coordinates that the telescope used to point for the first exposure of each observing sequence.

Appendix B: Tables of the Database

This section contains the description of the tables in the database. Following J-PLUS, measurements in different filters are shown as arrays. The order of filters is GSDSS, RSDSS, ISDSS, J0395, J0515, J0660, J0861. The labels of the filters have been capitalised to indicate that they are a label.

Table B.1. Content of the Objects table of the database

Column Name	Data Type	Unit	Description
obj_id	object	None	The J-PLUS object ID, with format {REF_TILE}-{NUMBER}; used for internal cross-matching with OBJ_ID in the Photometry Tables
ra	float64	deg	The RA of the object in the J-PLUS reference tile
dec	float64	deg	The DEC of the object in the J-PLUS reference tile
mean_ra	float64	deg	the mean RA position of all object detections in the J-VAR images
rms_ra	float64	deg	the RMS (actually NMAD) of MEAN_RA
mean_dec	float64	deg	the mean RA position of all object detections in the J-VAR images
rms_dec	float64	deg	the RMS (actually NMAD) of MEAN_DEC
mag_auto	object	mag	array of values of the J-PLUS photometry MAG_AUTO
mag_auto_err	object	None	array of values of the ERRORS of J-PLUS photometry MAG_AUTO
mag_aper_6	object	mag	array of values of the J-PLUS photometry MAG_APER_6 (6 arcsec aperture with aperture correction factor applied)
mag_aper_6_err	object	None	array of values of the ERRORS of J-PLUS photometry MAG_APER_6
mag_aper_3	object	mag	array of values of the J-PLUS photometry MAG_APER_3 (3 arcsec aperture with aperture correction factor applied)
mag_aper_3_err	object	None	array of values of the ERRORS of J-PLUS photometry MAG_APER_3
flags	object	None	array of SExtractor flags of the J-PLUS photometry
mask_flags	object	None	array of the flags obtained after applying masks on J-PLUS tiles during UPAD processing
single_det	object	None	array indicating whether an object is detected on the J-PLUS SingleMode SExtractor catalogue (0=no, 1=yes)
cls	float32	None	ClassStar assigned by SExtractor during photometry on the J-PLUS tile
mps	float32	None	Probability of being a star using the morphological method to classify the object (López-Sanjuan et al. 2019b)
sgc	float32	None	Probability of being a star by combining the available priors and classifications (López-Sanjuan et al. 2019b)
bannjos	object	None	Object classification via the BANNJOS algorithm (del Pino et al. in prep); classes are 'STAR', 'QSO', 'APS' (= Ambiguous Point Source)
fwhm	float32	None	Full Width at Half Maximum of the object on the J-PLUS reference (rSDSS) tile
morph_flag	int32	None	Additional Flag (0 or 1) to indicate potential issues with an object's morphology. A value of "1" is obtained when CLS < 0.3 or MPS < 0.3 or FWHM > 3 and it might be worth checking the object out
snr	object	None	Signal-To-Noise ratio of the J-PLUS photometry
hpix11	int32	None	Healpix index ORDER 11 (NESTED schema) of object position
ebv	float32	None	E(B-V) colour excess estimated from the Schlafly & Finkbeiner (2011) recalibration of the Schlegel, Finkbeiner & Davis (1998) dust map at infinity
ebv_err	float32	None	Error in the above E(B-V) value
vsx_var	int32	None	Flag to indicate whether or not the object is a known variable included in the VSX catalogue; 0=no, 1=yes
vsx_type	object	None	The VSX variable type classification of known variables; value is 'N/A' for all other objects
vsx_period	float64	None	The period (if available, otherwise period=0) of known variables; value is also 0 for all other objects
gaia_sid	int64	None	The <i>Gaia</i> DR3 source_id of the object; crossmatch radius is 1.1 arcsec, ID=0 if no match is found
gaia_xmulti	int32	None	Flag indicating the presence of multiple objects within the 1.1 arcsec crossmatch radius. Values are 0 if no, 1 if yes, -1 for unmatched objects. In case of multiple <i>Gaia</i> objects, the source_id assigned is the one corresponding to the smallest angular separation from the J-VAR object
gaia_prlx	float64	None	<i>Gaia</i> DR3 object parallax in mas; 'nan' if no parallax is available
gaia_prlx_err	float64	None	<i>Gaia</i> DR3 object parallax error in mas; 'nan' if no parallax is available
gaia_gmag	float64	None	The mean <i>Gaia</i> DR3 G magnitude (phot_g_mean_mag in gaia_source)
gaia_var	int32	None	Flag to indicate whether or not the object is classified as variable (phot_variable_flag in gaia_source). Values are 0 if no (GAIA=NOT_AVAILABLE), 1 if yes (GAIA=VARIABLE), -1 for unmatched objects
gaia_class	object	None	The <i>Gaia</i> classification of the variable (best_class_name in vari_classifier_result). There are <i>Gaia</i> objects flagged as 'VARIABLE' but without classification (in_vari_classification_result == False in vari_summary). These objects are assigned a 'NO_CLASS' value, while unmatched objects are assigned an 'N/A' value
gaia_score	float32	None	The score of the <i>Gaia</i> classification algorithm (best_class_score in vari_classifier_result). 'VARIABLE' objects with 'NO_CLASS' get a score=0, unmatched objects get a score=-1

Table B.2. Description of the columns of the Light Curves Table of the database

Column Name	Data Type	Unit	Description
obj_id	object	None	The J-PLUS object ID, with format REF_TILE-NUMBER
ra	float64	deg	The RA of the object in the J-PLUS reference tile
dec	float64	deg	The DEC of the object in the J-PLUS reference tile
hpix11	int32	None	Healpix index ORDER 11 (NESTED schema) of object position
field	int32	None	Number of the J-VAR field
filter	object	None	Name of the filter
mag	object	mag	The array containing the magnitudes
mag_err	object	None	The array containing the magnitude errors.
flags	object	None	array of SExtractor flags of the J-PLUS photometry; follows FORDER
fwhm	object	None	The array containing the FWHM value of the object in each image.
corr_curves	object	None	The array containing the curves used to calibrate each star's light curve
mjd	object	None	Corresponding MJD(UTC) value of the UTC timestamps.

Table B.3. Description of the columns of the Time Stamps table of the database

Column Name	Data Type	Unit	Description
field	int32	None	Number of the J-VAR field
filter	object	None	Name of the filter
utc	object	None	List with the dates and times of each of the images used for each measure of the object in a field and filter.
mjd	object	None	Corresponding MJD(UTC) value of the UTC timestamps.
imtype	object	None	a flag to keep track of the different images.

Table B.4. Description of the columns of the Photometry table of the database

Column Name	Data Type	Unit	Description
field	int32	None	Number of the J-VAR field
filter	object	None	Name of the filter
obj_id	object	None	The J-PLUS object ID, with format REF_TILE-NUMBER
cnum	int32	None	The number of comparison stars used to correct the object's light curve
sradius	float32	None	Search radius to encounter the above comparison stars
mag	object	mag	The array containing the magnitudes
mag_err	object	None	The array containing the magnitude errors.
flags	object	None	The array containing the photometric flags.
fwhm	object	None	The array containing the FWHM value of the object in each image.
corr_curves	object	None	The array containing the curves used to calibrate each star's light curve

Table B.5. Description of the columns of the SS0s_DETECTIONS table of the database.

Column Name	Data Type	Unit	Description
source_number	int32	None	None
catalog_number	int32	None	None
ra	float64	deg	None
dec	float64	deg	None
epoch	float32	None	None
mag	float32	None	None
magerr	float32	None	None
mag_aper	float32	None	None
mag_aper_err	float32	None	None
flux_aper	float32	None	None
flux_aper_err	float32	None	None
flux	float32	None	None
fluxerr	float32	None	None
pm	float32	None	None
pmerr	float32	None	None
pmra	float32	None	None
pmra_err	float32	None	None
pmdec	float32	None	None
pmdec_err	float32	None	None
mid_exposure_mjd	float32	None	None
date_obs	object	None	None
exptime	float32	None	None
matched	bool	None	None
skybot_number	float32	None	None
skybot_name	object	None	None
skybot_class	object	None	None
skybot_mag	float32	None	None
skybot_ra	float32	None	None
skybot_dec	float32	None	None
skybot_pmra	float32	None	None
skybot_pmdec	float32	None	None
skybot_deltara	float32	None	None
skybot_deltadec	float32	None	None
object	object	None	None
filter	object	None	None
ra_image	float32	None	None
dec_image	float32	None	None
image_filename	object	None	None
extension	float32	None	None
xwin_image	float32	None	None
ywin_image	float32	None	None
awin_image	float32	None	None
errawin_image	float32	None	None
bwin_image	float32	None	None
errbwin_image	float32	None	None
thetawin_image	float32	None	None
errthetawin_image	float32	None	None
erra_world	float32	None	None
errb_world	float32	None	None
errtheta_world	float32	None	None
flags_extraction	float32	None	None
flags_scamp	float32	None	None
flags_ima	float32	None	None
flags_ssos	float32	None	None
appid_object	object	None	None
mag_cal	float32	None	None
mag_cal_err	float32	None	None

Table B.6. Description of the columns of the SS0_magnitudes table of the database.

Column Name	Data Type	Unit	Description
ast_id	float32	None	ID of the SSO
ast_name	object	None	MPC name of the SSO
mag_j0395	float32	None	None
err_j0395	float32	None	None
mjd_j0395	float32	None	None
mag_gsdss	float32	None	None
err_gsdss	float32	None	None
mjd_gsdss	float32	None	None
mag_j0515	float32	None	None
err_j0515	float32	None	None
mjd_j0515	float32	None	None
mag_rsdss	float32	None	None
err_rsdss	float32	None	None
mjd_rsdss	float32	None	None
mag_j0660	float32	None	None
err_j0660	float32	None	None
mjd_j0660	float32	None	None
mag_isdss	float32	None	None
err_isdss	float32	None	None
mjd_isdss	float32	None	None
mag_j0861	float32	None	None
err_j0861	float32	None	None
mjd_j0861	float32	None	None
n_filters	int32	None	None